Journal of Geodynamics 107 (2017) 34–45

Contents lists available at ScienceDirect

Journal of Geodynamics

journal homepage: http://www.elsevier.com/locate/jog

# The December 2015 Mount Etna eruption: An analysis of inflation/deflation phases and faulting processes

Marco Aloisi [a,*], Shuanggen Jin [b,c], Fabio Pulvirenti [b], Antonio Scaltrito [a]

[a] Istituto Nazionale di Geofisica e Vulcanologia, Osservatorio Etneo, Catania 95125, Italy
[b] Shanghai Astronomical Observatory, Chinese Academy of Sciences, Shanghai 200030, China
[c] Department of Geomatics Engineering, Bulent Ecevit University, Zonguldak 67100, Turkey

ARTICLE INFO

*Article history:*
Received 17 October 2016
Received in revised form 27 February 2017
Accepted 5 March 2017
Available online 10 March 2017

*Keywords:*
GPS
Ground deformation modelling
Mount Etna
Coulomb stress changes
Inflation/deflation phases
Eruption

ABSTRACT

During the first days of December 2015, there were four paroxysmal events at the "Voragine" crater on Mount Etna, which were among the most violent observed during the last two decades. A few days after the "Voragine" paroxysms, the Pernicana – Provenzana fault system, located near the crater area, underwent an intense seismic swarm with a maximum "local" magnitude $M_L$ of 3.6. This paper investigates the relationship between the eruptive phenomenon and the faulting process in terms of Coulomb stress changes. The recorded seismicity is compatible with a multicausal stress redistribution inside the volcano edifice, occurring after the four paroxysmal episodes that interrupted the usual trend of inflation observed at Mt. Etna. The recorded seismicity falls within the framework of a complex chain of various and intercorrelated processes that started with the inflation preparing the "Voragine" magmatic activity. This was followed with the rapid deflation of the volcano edifice during the paroxysmal episodes. We determined that the recorded deflation was not the direct cause of the seismic swarm. In fact, the associated Coulomb stress change, in the area of seismic swarm, was of about −1 [bar]. Instead, the fast deflation caused the rarely observed inversion of dislocation in the eastern flank at the same time as intense hydrothermal activity that, consequently, underwent an alteration. This process probably reduced the friction along the fault system. Then, the new phase of inflation, observed at the end of the magmatic activity, triggered the faulting processes.



## 1. Introduction

Mount Etna, the largest volcano in Europe, is situated on continental crust and its formation is probably related to the nearby subduction process of the Ionian slab under the Tyrrhenian plate (Gvirtzman and Nur, 1999). The structural evolution of the volcanic edifice is the result of the action of volcanic sources combined with tectonic processes, characterized by the presence of important fault zones (Fig. 1). This study on a small part of this complex tectonic scenery will contribute to understanding how the movements between faults are related to each other and with magma dynamics. In particular, we estimated stress changes along the faults in the Pernicana – Provenzana fault system (Azzaro, 1999; Obrizzo et al., 2001; Palano et al., 2006; Guglielmino et al., 2011; Alparone et al., 2013) after the major eruptions occurring at the "Voragine" Crater (Fig. 1). This approach is supported by many authors (e.g., Patanè et al., 2005; Feuillet et al., 2006; Mattia et al., 2007; Currenti et al., 2008; Aloisi et al., 2011a; Bonanno et al., 2011; Privitera et al., 2012; Gonzalez and Palano, 2014) which share a common view that, at Mount Etna, the stress triggered by the magmatic activities is transferred to the faults and redistributed among them. For example, Feuillet et al. [2006], after analyzing historical earthquakes in eastern Sicily and eruptions at Mt. Etna volcano, found that volcanic sources and active faults are mechanically coupled. Therefore, there is evidence that magmatic and faulting processes can interact with each other by changing or perturbing the state of stress and, in turn, promoting or inhibiting earthquakes or eruptions. Moreover, it is well known that establishing the relationship between volcanic unrest at Etna and Pernicana fault system re-activation is a critical topic to understanding Etna mechanical behaviour (e.g., Currenti et al., 2012). In fact, the Pernicana – Provenzana fault system is one of the most active tectonic systems of Mt. Etna and it plays an important role in the dynamic of the eastern flank of the volcano, being closely correlated to the local stress field induced by volcano-related processes (Alparone et al., 2013).

* Corresponding author.
*E-mail addresses:* marco.aloisi@ingv.it (M. Aloisi), sgjin@shao.ac.cn (S. Jin), fabiopulvirenti@yahoo.it (F. Pulvirenti), antonio.scaltrito@ingv.it (A. Scaltrito).

http://dx.doi.org/10.1016/j.jog.2017.03.003
0264-3707/

It is known that, when earthquakes or magmatic activities occur, the stress state of the medium is modified by an additional stress field (e.g., Dragoni et al., 1982; Privitera et al., 2012), referred to as Coulomb static stress changes (hereafter, CSC). Earthquakes and volcanic activity interaction is a fundamental challenge for today's studies, leading to a deeper understanding of earthquake sequences, clustering and aftershocks. Many authors (e.g., Thatcher and Savage, 1982; Reasenberg and Simpson, 1992; King et al., 1994; Harris, 1998; Nostro et al., 1998; Stein, 1999; Hill et al., 2002; Marzocchi et al., 2002; Toda et al., 2002; Hyodo and Hirahara, 2004; Walter and Amelung, 2004; Feuillet et al., 2006; Calais et al., 2010; Xu et al., 2010; Toda et al., 2011; Pulvirenti et al., 2016) have demonstrated that the CSC quantity [measured in bar] can be regarded as an alteration of the "potentiality" of slip of the fault plane in response to the current stress state of the medium. In particular, when this quantity is positive, the movement on the fault plane is stimulated and earthquakes can be triggered. The minimum positive value of CSC to trigger an earthquake depends on the area where the fault is located because of the different rock properties. However, changes of about 0.1 bar are considered sufficient to trigger movements on the fault plane, when the system is close to the critical state of failure (e.g., Bonanno et al., 2011; Toda et al., 2011; Gonzalez and Palano, 2014; Pulvirenti et al., 2016).

In this paper, the relationship between the magmatic activities and the faulting process at Mount Etna is investigated in terms of CSC, in the area of the Pernicana – Provenzana fault system. We developed an analytical model to study the deformation pattern of the Etna volcano during the eruptive episodes occurring in December 2015. Therefore, the relationship between the inflation recorded prior to the magmatic activity, the sudden ensuing volcano deflation recorded during the December 2015 eruptive episodes, the starting of a subsequent new phase of inflation and the following faulting processes observed along the Pernicana – Provenzana fault system, are investigated in terms of CSC. Results indicated that, in a chain of various factors, only the new inflation phase following the eruptive episodes is correlated to positive Coulomb stress changes in the Pernicana – Provenzana fault system (Fig. 1), in accordance with the location, depth and focal mechanism of the recorded seismic swarm. In Section 2, the tectonic setting and 2015 eruption are introduced, a description of the recorded seismic activities and of the ground deformation modelling are presented in Sections 3 and 4, respectively, and, finally, discussions and conclusions are given in Sections 5 and 6.

## 2. Tectonic setting and December 2015 eruption

Mount Etna is a basaltic strato-volcano located in the eastern coast of Sicily (Italy). It lies along the front of the collision belt between the African and the Eurasian plates. Like many other volcanoes in the world (Ellis and King, 1991), Mount Etna has arisen from the flank of a normal fault, the Malta Escarpment. This is a major normal fault system separating the Hyblaean foreland from the thinned Ionian crust (Fig. 1). The Etnean volcanic activities have been interpreted as the result of extensional processes correlated a) to the Siculo-Calabrian rift zone (e.g., Ellis and King, 1991) or b) to vertical movement of asthenospheric material during the roll-back motion of the Ionian slab under the Tyrrhenian plate (e.g., Gvirtzman and Nur, 1999). The volcano is subject to a roughly N-S striking compressive regime due to the convergence between the Ionian and Tyrrhenian plates (e.g., Cocina et al., 1997; Barberi et al., 2000) and, contemporaneously, to an extensional approximately WNW-ESE regime, associated to the Malta Escarpment dynamics (e.g., Ellis and King, 1991; Hirn et al., 1997). Moreover, the volcanic edifice is also subject to the local stress due to magma activities (e.g., Barberi et al., 2000). The interaction between this very articulated stress field at Mount Etna produces two kinematically distinct sectors: a) the western flank that has scant morphological evidence of faulting or eruptive fracturing and, analyzing the recorded ground deformation pattern, is a clear indicator of the volcano inflation/deflation phases, and b) the eastern flank that is formed by several fault systems accommodating a near constant seaward flank displacement whose origin is still fiercely debated (e.g., Palano et al., 2008; Palano et al., 2009; Aloisi et al., 2011a; Chiocci et al., 2011; Cannavó et al., 2014; Mattia et al., 2015; Palano, 2016).

Mount Etna is characterized principally by two types of eruptions (e.g., Aloisi et al., 2009): a) summit strombolian eruptions, where magma intrudes through the central conduit system, and b) dike-forming eruptions, when magma breaks out at the surface, bypassing the central conduit system. Historically, most of the dike-forming intrusions ascend along two rift zones, a) the NE Rift and b) the S Rift zone (Fig. 1). In this paper, we discuss the summit eruptions occurring in December 2015 and their relationship with the following seismic activity recorded at the northern end of the NE Rift, along the Pernicana – Provenzana fault system.

Starting from the 2nd of December 2015, four intense paroxysmal eruptive episodes occurred at the central crater, known also as "Voragine" crater (Fig. 1). The volcanic activity was characterized by tall lava fountains and by eruption columns, several kilometres high. $SO_2$ emissions, related to the different paroxysms, were tracked above the eastern Mediterranean, Syria, Iraq and China areas. The paroxysmal events were among the most violent to be observed at Mount Etna during the last two decades.

In the past, the "Voragine" crater underwent two particularly intense paroxysms on 22 July 1998 and on 4 September 1999, with similar characteristics to those of the paroxysms recorded during December 2015 (https://www.volcanodiscovery.com/italysvolcanoes/VOR95_99.html). In particular, the episode in July 1998 was accompanied by fire-fountaining and tephra emission. Successively, vigorous activity at the Voragine resumed in early August, with another paroxysmal eruptive episode on the 6th. After this volcanic episode, the Voragine became active again in June 1999. From then on, the activity gradually increased, culminating in another paroxysm on 4 September 1999, similar but more violent to that of 22 July 1998. Successively, the Voragine experienced several further episodes of vigorous activity during the weeks following the 4 September 1999 eruption, but none were of similar magnitude. Finally, further violent paroxysmal episodes took place at the "Voragine" crater in February 1947, July-August 1960 and August 1989.

Concerning recent activity, there were modest and sporadic ash emissions at the "Voragine" crater from August 2015. More significant volcanic activity started during the month of October 2015, when the opening of a vent, producing modest intra-crateric strombolian activities and sporadic weak ash emissions, was observed. This activity continued during October and November without substantial variations, although it showed an increase in frequency and intensity over time. Since the 1st of December until about 13:00 UTC on the 2nd of December, the volcanic tremor, namely the daily average of the Root Mean Square (RMS) amplitude of the vertical component of seismic signal (e.g., McNutt, 1991; Alparone et al., 2003; Di Grazia et al., 2006), showed temporary episodes of unrest with oscillations in amplitude (Fig. 2 a). The intra-crateric strombolian activity became intense and recurrent. Successively, the volcanic tremor increased progressively (Fig. 2a), culminating during the first hours of the 3rd of December, at about 02:20 UTC, with a violent paroxysmal episode that lasted approximately 40 min. The volcanic activity consisted of tall lava fountains, some hundreds of meters high, and by an eruption column about 10 km high (above the sea level). At the end of the first paroxysmal event, the strombolian activities inside the "Voragine" crater continued.

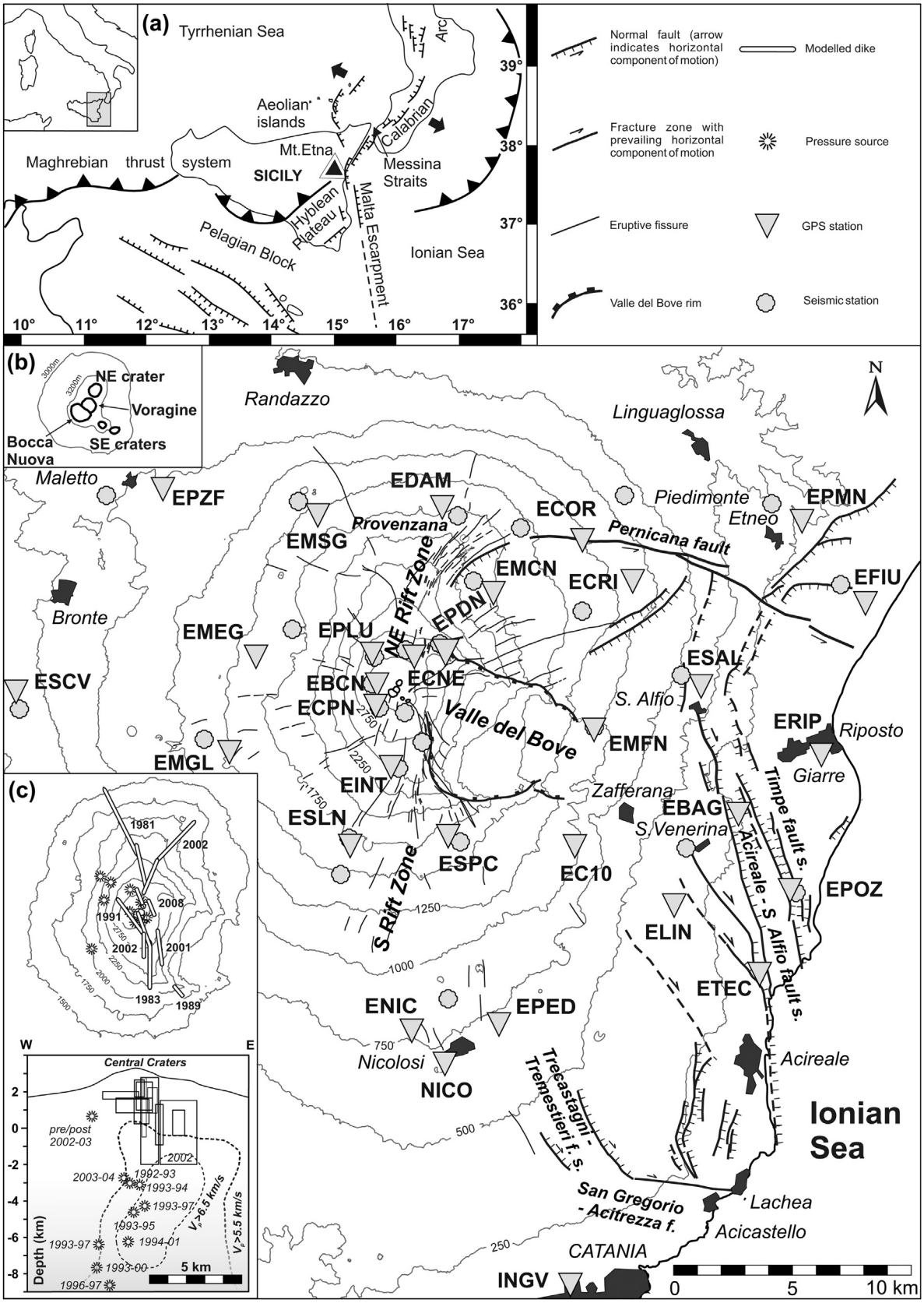


**Fig. 1.** Map of Mount Etna with the continuous CGPS network (inverted triangles) and seismic network (circles), run by INGV-OE. A sketch map of the fault systems is reported, together with the NE and South rift zones. In the inset a), the location of Mount Etna in the central Mediterranean area is shown at the footwall of the Malta Escarpment. In the inset b), the crater area is shown in detail. The inset c) shows the consensus magma pathways, as historically resolved by GPS, seismic, and other geophysical data. Redrawn from Aloisi et al. (2011a).

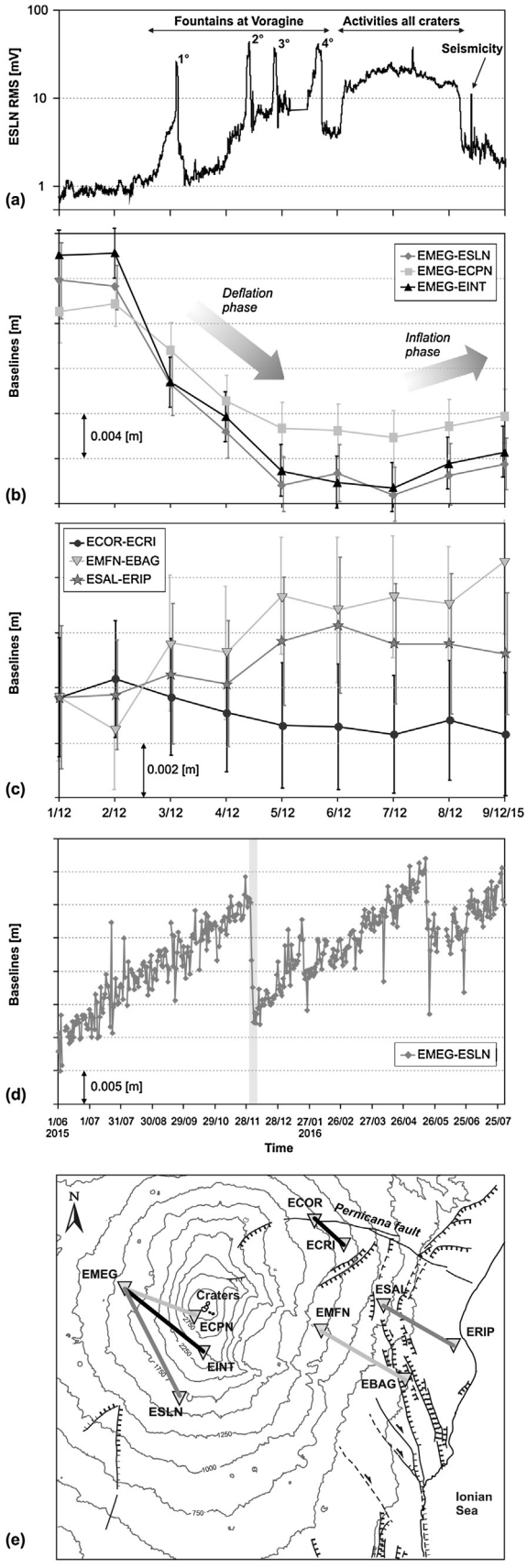


**Fig. 2.** (a) RMS of the seismic signal recorded at the ESLN station from 1 to 9 December 2015. (b) Length variation of three CGPS baselines (EMEG-ESLN, EMEG-ECPN, EMEG-EINT) located in the western flank of Etna volcano, from 1 to 9 December. (c) Length variation of one CGPS baseline (ECOR-ECRI) located across the Pernicana fault, from 1 to 9 December. The data clearly show the sudden variations related to the fast deflation recorded during the four paroxysms (from 2 to 6 December). The starting of a new phase of inflation during 7–8 December can also be seen. Two CGPS baselines (ESAL-ERIP and EMFN-EBAG) located on the eastern flank are also reported. (d) Length variation of the CGPS baseline EMEG-ESLN for a long period (from June 2015 to July 2016). (e) Map of Mount Etna showing the plotted baselines.

Weak ash emissions were observed at the New Southeast Crater (NSEC) and at the North-East crater (NEC), see inset b) in Fig. 1. A few hours later, at about the 09:00 UTC on the 4th of December, the "Voragine" crater underwent a second paroxysmal episode (Fig. 2a), lasting as long as the first episode. During this paroxysm, there were frequent ash emissions at the NSEC. The volcanic tremor amplitude remained high at the ESLN seismic station (Fig. 2a). It reached a peak during the second paroxysm in the morning, which was higher than the peak associated with the paroxysm of the 3rd of December. At about 20:35 UTC on the 4th of December and at about 14:55 UTC on the 5th of December, the "Voragine" crater underwent two more intense eruptive episodes. These two episodes had similar features and durations as the first two eruptive paroxysms. Successively, the eruptive activity at the "Voragine" crater gradually diminished. The ash emissions continued at the NSEC. At the end of the fourth paroxysmal episode, the volcanic tremor amplitude remained high (Fig. 2a), for about 7 h, when, at about 01:00 UTC on the 6th of December, it increased rapidly. During this new phase, the volcanic tremor amplitude remained almost constantly high during the time, until about 06:00 UTC on the 8th of December. This phase was characterized by vigorous strombolian and effusive activities at the NSEC. The NSEC was also affected by ash emission. As described before, from the 3rd of December, weak ash emission has been observed at the NSEC and at the NEC. From the 7th of December, the NEC was affected by sporadic strombolian activity. This phase ended on the 8th of December at about 05:00 UTC, when the volcanic tremor amplitude sharply decreased to roughly the value reached after the fourth "Voragine" crater paroxysms (Fig. 2a). During the first hours of the 8th of December, also the NSEC eruptive activity decreased rapidly together with the volcanic tremor amplitude but, contemporaneously, the ash emissions at the NEC increased. During this last phase, the volcanic tremor amplitude decreased slowly together with the observed volcanic activity. In particular, there was a new increase of ash emission at the NEC during December 9–11. Finally, sporadic ash emissions and weak explosive activities were observed at the "Voragine" crater, NSEC and NEC until the end of December.

## 3. Seismic activities in december 2015

The Etna Permanent Network, managed by Istituto Nazionale di Geofisica e Vulcanologia, Osservatorio Etneo (INGV-OE), consists of 35 three-component digital seismic stations (Fig. 1). These stations are equipped with broadband (Trillium–Nanometrics, $F_n = 40$ s) three-component sensors, with a dynamic range of 144 dB. Data are acquired and recorded locally with a digital frequency of 100 Hz, using the Nanometrics Trident Digital Systems (24 bits). These data are transmitted via satellite or radio to the data acquisition center of the INGV-OE, Catania. All the stations use the same base time, set by GPS time.

Earthquakes at Mt. Etna can be divided in two major groups: a) volcanic-tectonic earthquakes that are generated by regional tectonic stress, local stress induced by dike-forming intrusion, local stress due to slower inflating sources or by a mutual interaction between the previously described causes (e.g., Patanè et al., 2003; Gambino, 2016); b) long-period events driven by stress changes caused by an intermittent degassing process occurring at depth (e.g., Cauchie et al., 2015). Usually, volcanic-tectonic earthquakes

**Table 1**
Main hypocentral parameters of the localized events.

| N | Date | Origin Time | Lat | Long | Depth [km] | $M_L$ | Area |
|---|---|---|---|---|---|---|---|
| 1 | 07/12/2015 | 19.12.20 | 37.8079 | 15.0510 | 0.02 | 2.6 | 1.8 km W from Piano Pernicana (CT) |
| 2 | 08/12/2015 | 09.28.30 | 37.8037 | 15.0453 | 1.26 | 3.6 | 1.5 km E from Monte Nero (CT) |
| 3 | 08/12/2015 | 09.32.03 | 37.8125 | 15.0538 | 0.82 | 2.7 | 1.7 km W from Piano Pernicana (CT) |
| 4 | 08/12/2015 | 09.36.22 | 37.8113 | 15.0455 | 0.93 | 2.3 | 1.4 km E from Monte Nero (CT) |
| 5 | 08/12/2015 | 09.56.00 | 37.8039 | 15.0412 | 1.11 | 1.7 | 1.2 km SE from Monte Nero (CT) |
| 6 | 08/12/2015 | 10.22.37 | 37.8021 | 15.0395 | 1.24 | 1.4 | 1.2 km SE from Monte Nero (CT) |
| 7 | 08/12/2015 | 10.53.54 | 37.8024 | 15.0434 | 1.5 | 3.2 | 1.4 km SE from Monte Nero (CT) |
| 8 | 08/12/2015 | 14.55.57 | 37.7968 | 15.0278 | 1.29 | 1.3 | 1.4 km S from Monte Nero (CT) |
| 9 | 08/12/2015 | 20.06.25 | 37.8081 | 15.0462 | 0.36 | 2.1 | 1.4 km E from Monte Nero (CT) |
| 10 | 08/12/2015 | 20.50.37 | 37.8028 | 15.0415 | 1.98 | 1.3 | 1.3 km SE from Monte Nero (CT) |
| 11 | 08/12/2015 | 20.51.15 | 37.8077 | 15.0555 | 1.22 | 1.6 | 1.4 km W from Piano Pernicana (CT) |
| 12 | 09/12/2015 | 01.27.09 | 37.8020 | 15.0365 | 1.11 | 1.2 | 1.0 km SE from Monte Nero (CT) |
| 13 | 09/12/2015 | 08.14.29 | 37.8078 | 15.0429 | 1.05 | 2.1 | 1.2 km E from Monte Nero (CT) |
| 14 | 10/12/2015 | 04.43.29 | 37.7973 | 15.0296 | 1.55 | 1.6 | 1.3 km S from Monte Nero (CT) |

**Table 2**
Estimated focal parameters (numeration from Table 1).

| N | Date | Origin Time | Lat | Long | Depth [km] | $M_L$ | Strike | Dip | Rake | Area |
|---|---|---|---|---|---|---|---|---|---|---|
| 1 | 07/12/2015 | 19:12:20 | 37.8079 | 15.0510 | 0.02 | 2.6 | 170 | 60 | −160 | 1.8 km W from Piano Pernicana (CT) |
| 2 | 08/12/2015 | 09:28:30 | 37.8037 | 15.0453 | 1.26 | 3.6 | 80 | 55 | −10 | 1.5 km E from Monte Nero (CT) |
| 3 | 08/12/2015 | 09:32:03 | 37.8125 | 15.0538 | 0.82 | 2.7 | 60 | 65 | −60 | 1.7 km W from Piano Pernicana (CT) |
| 4 | 08/12/2015 | 09:36:22 | 37.8113 | 15.0455 | 0.93 | 2.3 | 95 | 70 | −30 | 1.4 km E from Monte Nero (CT) |
| 7 | 08/12/2015 | 10.53.54 | 37.8024 | 15.0434 | 1.5 | 3.2 | 90 | 55 | −50 | 1.4 km SE from Monte Nero (CT) |

occur mainly in the form of swarms, seldom exceeding magnitude 4 (Gambino, 2016).

Fig. 3 shows the seismicity recorded between August and December 2015. This seismicity belongs to the volcanic-tectonic typology and affected mostly the eastern sector of the volcano edifice. It is grouped in swarms in the area of Pernicana – Provenzana faults system, located near the crater area, and in the eastern flank, near the area of Zafferana town (Fig. 3). We focused on an intense seismic swarm occurring in the uppermost segment of the Pernicana – Provenzana fault system (Fig. 3 and inset). In particular, between the 7th and 10th of December 2015, about 100 earthquakes with local maximum magnitude $M_L$ of 3.6 were recorded in this area. The swarm started with an event of $M_L$ 2.6, on 7 December, but the main earthquakes took place in the morning of 8 December, with two events at 09:28 GMT ($M_L$ = 3.6) and at 10:53 GMT ($M_L$ = 3.2). Only 14 events of the swarm were located, since the low level of recorded magnitude rarely exceeded the value of $M_L$ = 2.0 (see inset in Fig. 3 and Table 1). The depth of the swarm was between 0 and 1.5 km, below the sea level.

Fig. 4 shows the daily earthquake rate and the associated cumulative strain release (e.g., Alparone et al., 2015) of the earthquakes located during the period 2014–2015. It is noteworthy that the Pernicana – Provenzana 2015 swarm produced the main seismic energy release during the last two years, on Mount Etna (Fig. 4a). Moreover, between August and December 2015, another minor swarm occurred in the area of Milo – Zafferana towns (Fig. 4b).

The events belonging to the Pernicana – Provenzana 2015 swarm were selected from the INGV-OE catalogue (Gruppo Analisi Dati Sismici, 2016). The earthquakes were located using the Hypoellipse code (Lahr, 1989) and the 1D crustal velocity model proposed for Etna area by Hirn et al. (1991). We also computed the focal mechanisms for five earthquakes (Fig. 3 and Table 2). To this end, we selected only those events with at least ten first motion P-polarities and with sufficient station coverage on the focal sphere. We used the FPFIT code by Reasenberg and Oppenheimer (1985). The focal mechanism of the main earthquake had the following parameters: strike 80°, dip 55°, rake −10°. Overall, the fault-plane solutions showed (Fig. 3) a trans-tensional faulting feature, with P-axes roughly NE-SW oriented and dipping from 30° to 59°. These focal mechanisms have a near EW striking nodal plane roughly resembling the geological fault traces along the Provenzana – Pernicana fault system. Our results were in agreement with other literature data (Barberi et al., 2004; Alparone et al., 2013) and with field observations.

## 4. Deformation observations and modelling

Continuous GPS (hereafter, CGPS) monitoring of ground deformations on Mt. Etna started in November 2000. The current network configuration includes 33 stations that cover the entire volcano edifice (Fig. 1). CGPS data collected by the Etnean network were processed with the GAMIT/GLOBK software with IGS (International GNNS Service) precise ephemerides and Earth orientation parameters from the International Earth Rotation and Reference Systems Service (IERS), (King and Bock, 2004; Jin and Park, 2006). The precise baselines with uncertainty are obtained on a daily based solution.

We analyzed the CGPS data collected at Mt. Etna from June 2015 to July 2016, focusing in detail on December 2015, when Mt. Etna was undergoing intense volcanic and seismic activities. The December 2015 events occurred during the usual trend of volcano inflation (Fig. 2d). In particular, the increase in length of the baseline EMEG-ESLN showed clearly how the dynamic of the volcano inflation was active several months before the volcanic episodes. Conversely, during the four paroxysmal eruptive episodes occurred at the "Voragine" crater, from the 2nd to the 6th of December, the continuous CGPS network recorded a rapid deflation of the volcano that affected the entire edifice (Figs. 2d; 5a and b). It is noteworthy that this trend is evident also at the ECRI station (Fig. 2c and 5a and b). The ECRI station usually shows a horizontal movement toward East, in line with the dynamics of the near Pernicana fault, whereas, during the paroxysmal episodes and following the overall volcano deflation, the station showed a dislocation roughly toward South-West and the baseline ECOR-ECRI decreased in length (Fig. 2c). Successively, from the 7th of December, a new phase of inflation started (Fig. 2b–d), with a similar trend to the usual inflation affecting the volcano before the eruptive episodes (Fig. 2d).

We modelled the recorded deformation pattern associated with the rapid deflation phase, occurring between the 2nd and the 6th of December (Figs. 2 and 5), as induced by a pressure source acting

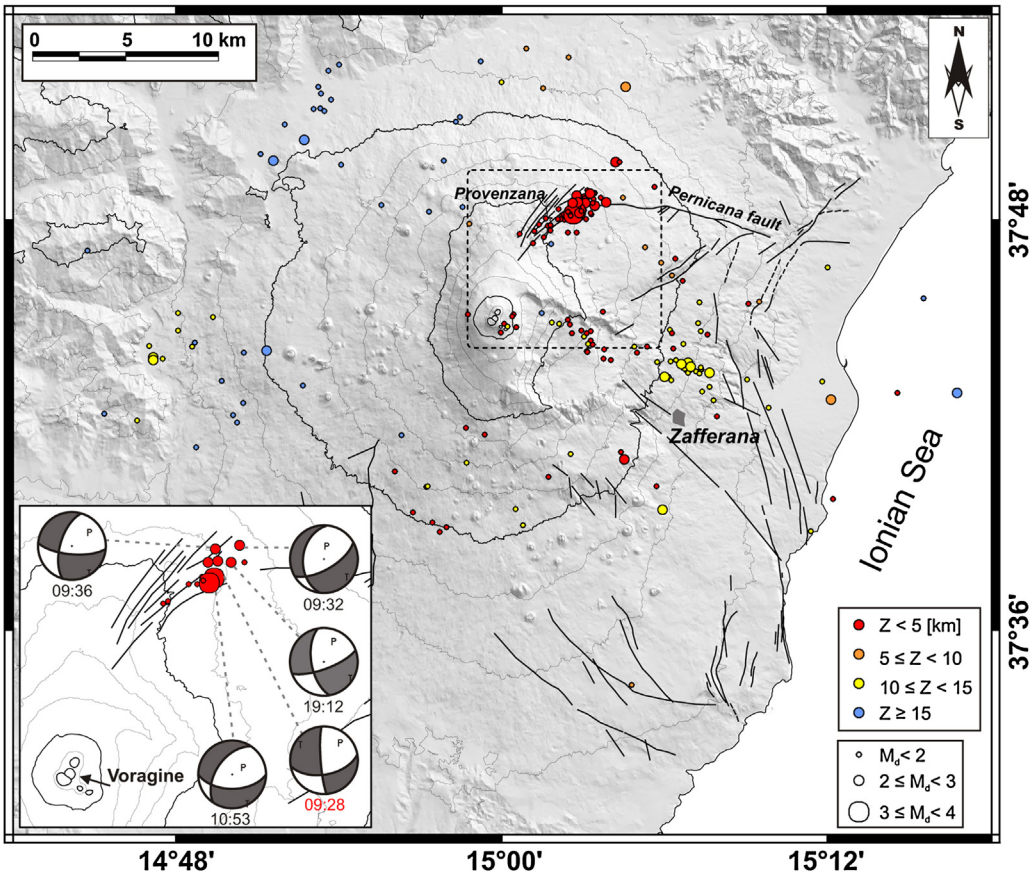


**Fig. 3.** Spatial distribution of the seismicity recorded between August and December 2015. In the inset, the 2–10 December seismicity and the principal focal mechanisms are shown.

inside the volcano. We used the entire CGPS network but we set a lower weight at the ECPN and EC10 stations because, in this case, they were both affected by local effects or instrumental errors. We performed an analytical inversion of CGPS data, assuming the pressure source as a finite spherical magma body solution of McTigue (1987), obtaining a plausible data fit (Fig. 5). Among the different analytical models published in literature, we chose this source model since it showed a good trade-off between the number of degrees of freedom and the obtained data fit. Moreover, unlike the inflation sources characterized by an elongated shape, deflation sources typically showed an almost spherical shape (Bruno et al., 2012). We therefore retain that, in this case, a spherical source can represent the recorded deformation pattern well. The McTigue (1987) pressure source is determined by five parameters: the coordinates "$x_c$", "$y_c$" and "$z_c$" of the sphere center, the radius "r" and the pressure "P" on the surface of the model. It is well known that there is a trade-off between the crustal strength, the source pressure and the related volume (e.g. Davis, 1986; Yang et al., 1988; Newman et al., 2006). Hence, we might obtain a considerable uncertainty on the estimation of source pressure if we do not know the correct material properties and plausible source volume. In order to estimate the model parameters, we performed an analytical inversion using the Genetic Algorithm (Goldberg, 1989) and, subsequently, the Pattern Search technique (Lewis and Torczon, 1999) and a Non-linear Least Squares technique. To estimate the uncertainty of each optimized model parameter, we adopted a Jackknife re-sampling method (Efron, 1982). We included the effects of the topography using the topographically corrected method of Williams and Wadge (2000). The medium was supposed homogeneous and isotropic with a Young modulus of 75 GPa and a Poisson ratio of 0.25 (Aloisi et al., 2011a).

**Table 3**
Model parameters and related uncertainties. ΔV is calculated according to Tiampo et al. (2000) using a value of the effective shear modulus μ equal to 5 GPa.

| | |
|---|---|
| $x_c$ [m] | $499604 \pm 85$ |
| $y_c$ [m] | $4178354 \pm 102$ |
| $z_c$ [m] | $-4840 \pm 248$ |
| r [m] | $288 \pm 69$ |
| P [Pa] | $-1.3 \times 10^9 \pm 2.5 \times 10^7$ |
| ΔV [$m^3$] | $-20 \times 10^6 \pm 15 \times 10^6$ |

The final optimal solution for the deflation phase is shown in Fig. 5(c and d) and the parameters are reported in Table 3. The obtained source is located under the "Voragine" crater, where the four paroxysms occurred, at a depth of about 4.8 km, below the mean sea level. We calculated the volume change ΔV (Table 3) according to Tiampo et al. (2000), using a suitable value of the effective shear modulus μ for a hot volcanic region equal to 5 GPa (e.g., Bonafede et al., 1986; Davis, 1986; Bonaccorso et al., 2005). We obtained a variation in volume of about $-20 \times 10^6$ $m^3$ of magma for all the four paroxysms. It is noteworthy that the position of the December 2015 deflation source is compatible with the historical solutions found in literature (e.g., Aloisi et al., 2011a; Bruno et al., 2012). In particular, the deflation pressure sources are usually located along the western border of the high velocity zone found by Aloisi et al. (2002), just below the Central Crater area (Bruno et al., 2012). This position is compatible with the path where the magma is thought to ascend, according to tomographic analysis (e.g., Aloisi et al., 2002). Regarding the found depth of about 4.8 km below the mean sea level, this level is of primary importance because, consid-

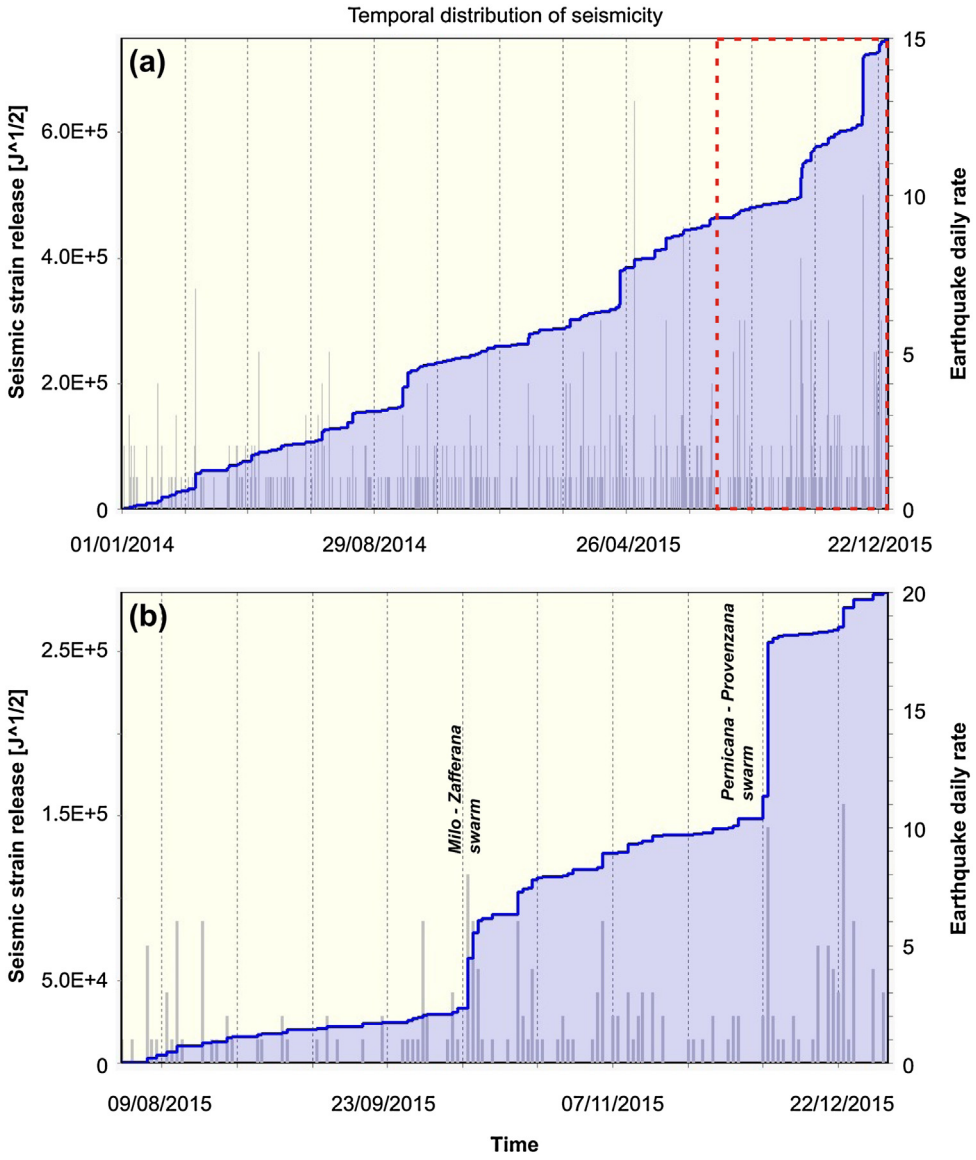


**Fig. 4.** Number of earthquakes per day (grey bars) and cumulative curve of seismic strain release (blue line) associated to the period 2014–2015 (a) and a detail (dashed red line) relative to the period between August and December 2015 (b). (For interpretation of the references to colour in this figure legend, the reader is referred to the web version of this article.)

ering its depth beneath the crater area (about 7 km), it corresponds approximately to the pressure of exsolution (180 MPa) and bubbles formation of Etnean magmas with a normal content in water (2%), (see Bruno et al., 2012).

## 5. Eruptive process and discussions

In this paper, we investigated the interaction between the volcanic sources at Mt. Etna and the active faults in terms of mechanical coupling, by examining how the perturbation of the state of stress can promote or inhibit the seismicity. Taking into account the fault location, geometry and rake for the 8th of December recorded seismicity, we analyzed the relationship between the "Voragine" 2015 magmatic activities, the prior inflation phase, the following inflation phase and the faulting process, in terms of CSC.

Taking into account the estimated focal mechanism for the mainshock, recorded on the 8th of December at 09:28 UTC ($M_L = 3.6$), we calculated the CSC induced by the modelled deflation source. We found that the movement on the fault plane along the Pernicana – Provenzana system is clearly discouraged (Fig. 6). This means that the deflation phase, produced by the four paroxysmal episodes at the "Voragine" crater, is not the direct cause of the seismic swarm recorded a few days after. By contrast, a direct link between volcanic and seismic activity has been demonstrated in other cases. For example, the seismic swarm occurring on the southeastern flank of Mt. Etna on the 9th of January 2001 was associated with the magmatic recharge preceding the Mt. Etna 2001 eruption (Gambino, 2016). Also the 22 September 2002 Pernicana seismicity was associated with a tensile mechanism occurring during the magma intrusion that preceded the lateral eruption a month later (Currenti et al., 2012). The October 2002 Pernicana seismic swarm was directly correlated to the dyke-forming intrusions occurring during the 2002–2003 Mt. Etna eruption (Pulvirenti et al., 2016). As in our case, there was not always a direct link between volcanic and seismic activity. For example, the 2–3 April 2010 Pernicana seismic swarm was associated with the flank seaward movement, extending the eastern sector of Mt Etna (Currenti

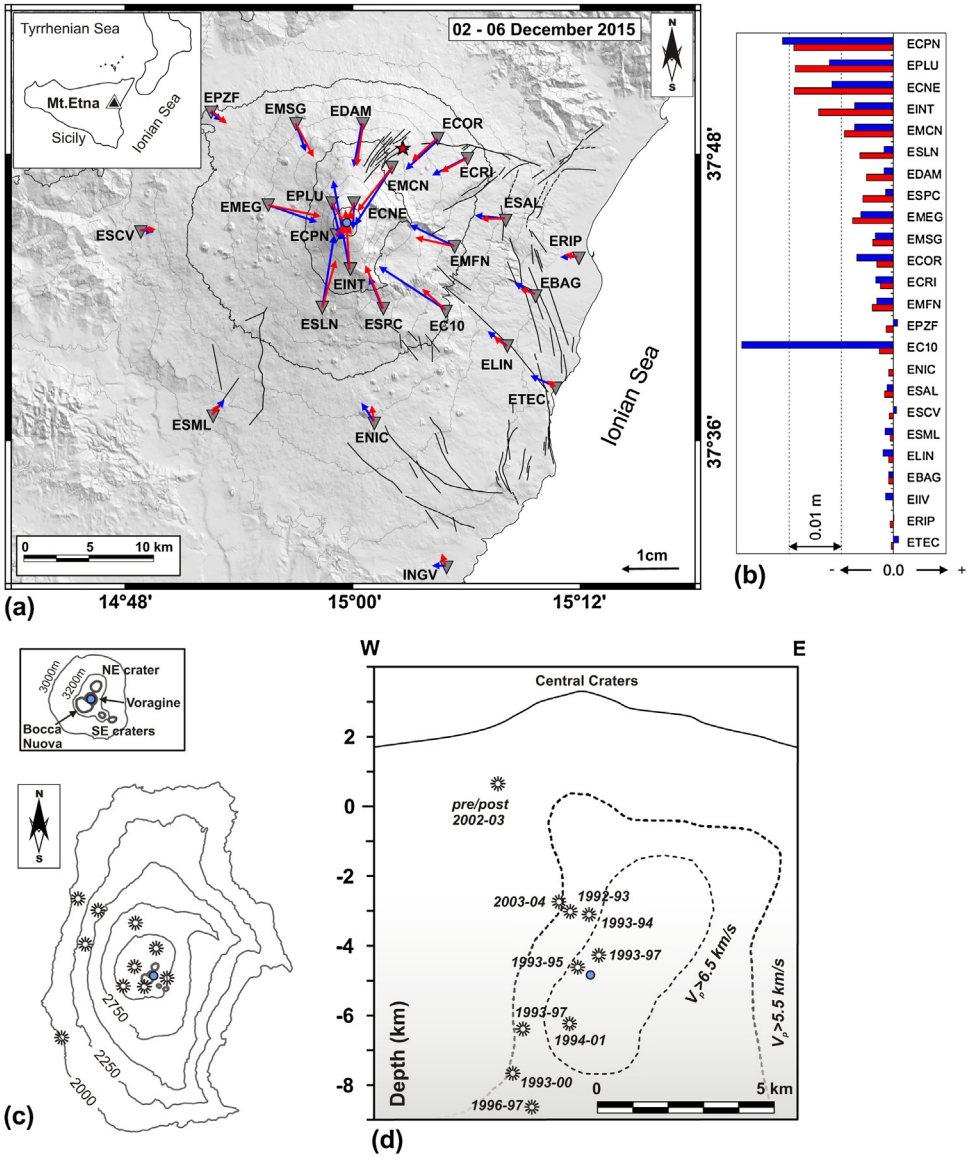


**Fig. 5.** a) Recorded (blue arrows) and modelled (red arrows) horizontal displacement field from 2 to 6 December. The mean uncertainty is of about 2.0–2.3 [mm]. b) The histogram reports the recorded (blue bars) and modelled (red bars) vertical dislocations. The vertical variations are sorted by the CGPS station elevations. The position of the modelled volcanic source in deflation (cyan circle) is also reported in horizontal c) and vertical d) projection. The red star in a) indicates the main earthquake recorded during 8 December 2015. The consensus magma pathways (black asterisks) as historically resolved by GPS, seismic and other geophysical data are indicated in c) and d) (see Aloisi et al. (2011a) for an overview). The trace of the high $v_p$ body estimated by Aloisi et al. (2002) is also shown in d). (For interpretation of the references to colour in this figure legend, the reader is referred to the web version of this article.)

et al., 2012). Therefore, we think that the December 2015 seismicity can be interpreted exclusively in the framework of a significant interplay between various processes (Fig. 7).

Although almost within the limit of instrumental errors, it is worth noting that the baseline ECOR-ECRI (Fig. 2c) showed an inversion of the usual kinematics during the paroxysmal episodes. The length of the baseline ECOR-ECRI usually increases in time, according to the dislocation along the Pernicana fault. Instead, during the "Voragine" eruptive episodes, the baseline decreased in length. Therefore, we believe that the four violent paroxysms destabilized the area subject to the seismic swarm.

Moreover, on examining three typical CGPS baselines (Fig. 2b), we can observe that, during the four eruptive episodes and all crater activities, the CGPS network recorded a deflation (the baseline length decreases). However, starting from the 7th of December, one day before the main earthquake of the seismic swarm, the CGPS baselines began increasing in length. This means that the CGPS network started to record a new typical inflation phase (Fig. 2d), very similar to the phase of inflation that the volcano recorded before the "Voragine" eruptive episodes. In order to explain this inflation, we can observe that the seismic tremor, just a few hours before the seismic swarm, decreases rapidly (Fig. 2a). We assumed, after the four paroxysmal episodes at the "Voragine" crater and the activities observed at the NSEC and NEC craters, that the modelled deflation area located at a depth of about 4.8 km (below the mean sea level) and the entire overlying plumbing system were filled with less volatile-rich magma than the one erupted before. This observation, that corresponds to the decreasing concentration of dissolved volatiles and of the gas boiling, can explain the rapid drop in seismic tremor and the progressive decreasing of the observed volcanic activity. The volatiles that continuously rise through the magmas (Ferlito et al., 2009; Ferlito and Lanzafame, 2010), in the plumbing system, therefore now characterized by a low concentration of dissolved volatiles, can explain the beginning

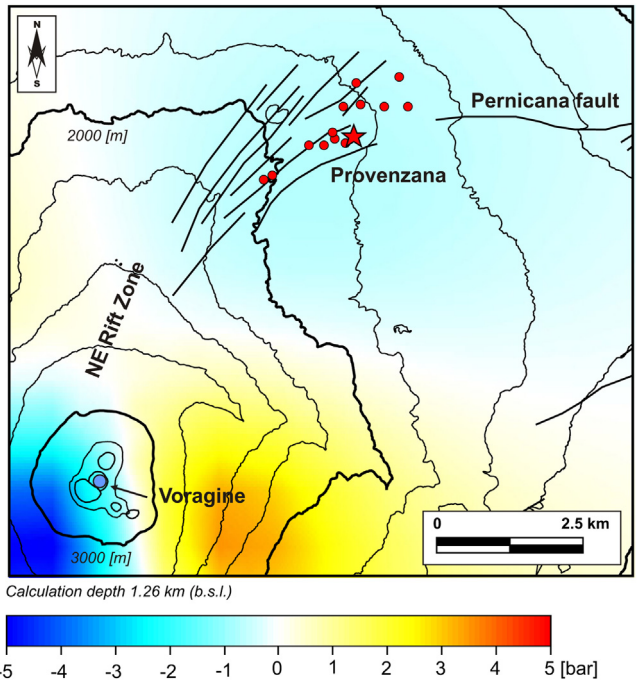


**Fig. 6.** Map of the Coulomb stress changes induced by the modelled deflation source and resolved on the receiver fault strike (80°, dip 55°, rake −10°) estimated for the mainshock (8th of December at 09:28 UTC, $M_L = 3.6$), at the depth of 1.26 km (b.s.l.), namely the hypocentral depth of the earthquake. The star indicates the main recorded earthquake ($M_L = 3.6$) and the cyan circle the modelled volcanic source. The seismic swarm is also reported (red circles).

of the new phase of inflation. Our hypothesis here is that the content of volatiles in the new batch of magma, that filled the deflation area and the overlying plumbing system, increased in time after the eruptive activity, promoting the new inflation phase (Fig. 2d). In particular, we believe that the observed overpressure provided to the magma is associated to the gas exsolution and boiling. It is not possible to model the source of inflation between 7th and 8th of December, because we recorded very small displacements at the CGPS network, just beyond the instrumental error. The observed overpressure during one day was very small. If we hypothesize a positive variation in volume located at about 4.8 km, below the mean sea level, roughly matching with the depth and horizontal position of the previous source in deflation producing the here modelled 2015 "Voragine" volcanic activity, we obviously obtain positive CSC in correspondence with the recorded seismicity along the Pernicana – Provenzana fault system. Therefore, the recorded earthquakes could be compatible with the starting of a new phase of inflation and, probably, the previous rapid deflation produced a state of disequilibrium in the studied area (Fig. 7). Likewise, as aforementioned, the seismic swarm on the southeastern flank of Mt. Etna on the 9th of January 2001 represented a shear response to a local stress caused by the magmatic recharge preceding the Mt. Etna 2001 eruption (Gambino, 2016). It was determined that the 9th of January fault reactivation occurred along pre-existing structures, most likely, because of the presence of fluids. In fact, Siniscalchi et al. (2012), by means of magnetotelluric survey on the eastern flank of Mt. Etna, have detected several high conductivity zones, suggesting diffuse hydrothermal activity and fluid circulation. In particular, the authors deduced that the zone with the strongest conductivity lies in the intensely fractured hanging wall of the Per-

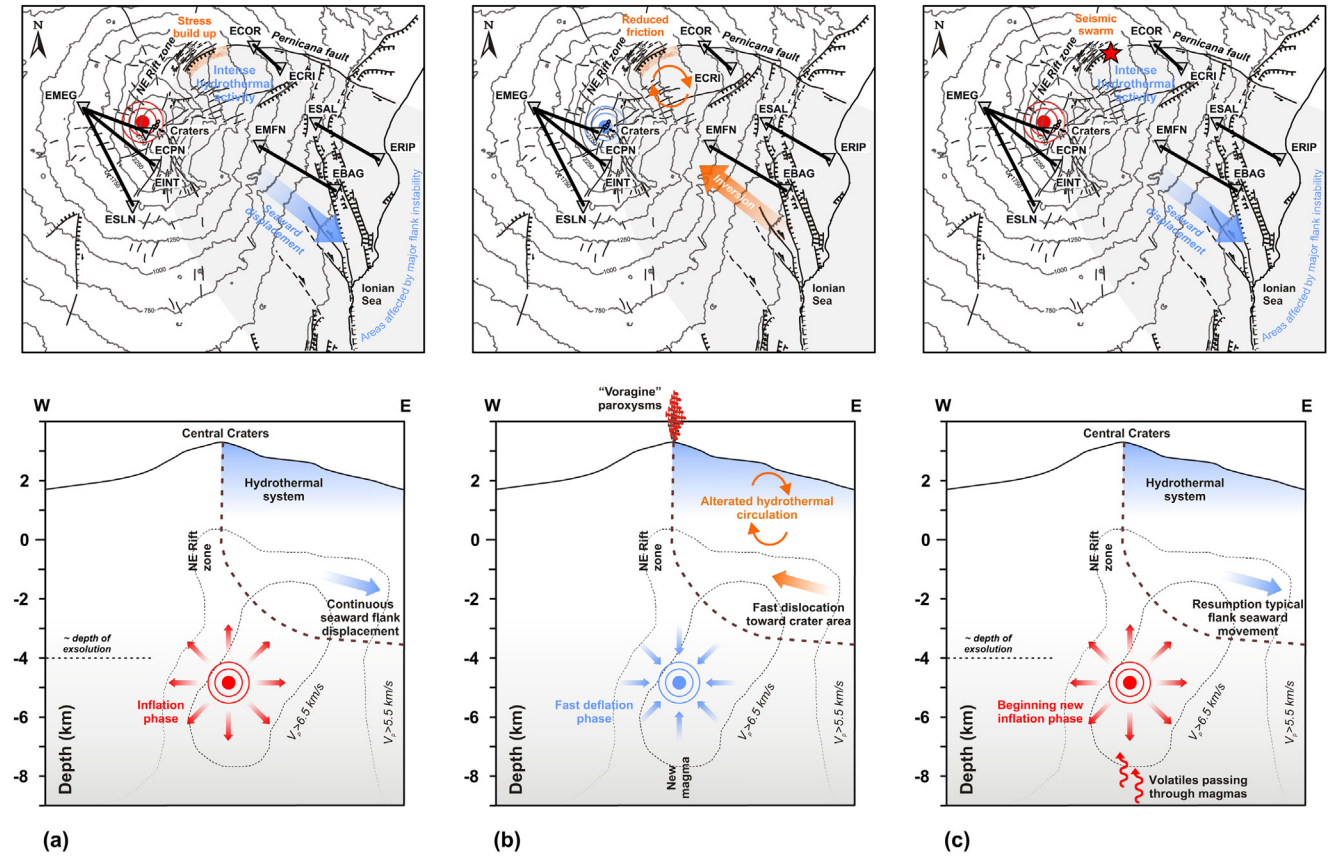


**Fig. 7.** Sketch map showing the volcanic and tectonic processes leading to the 2015 December seismic activity. a) Inflation phase recorded before the "Voragine" paroxysmal episodes, from June 2015 until the 2nd of December 2015. b) "Voragine" paroxysmal episodes, from 2 to 6 December 2015. c) Onset of a new phase of inflation, promoting the faulting processes, from 7 to 10 December 2015.

nicana fault system (see also Siniscalchi et al., 2010). Therefore, the area where the December 2015 swarm occurred is affected by intense hydrothermal activity, fluid circulation and convective hydrothermal cells, able to induce instability (Fig. 7). During the "Voragine" magmatic activity – among the most violent observed during the last two decades – the entire eastern flank, that is usually characterized by a continuous seaward movement (Fig. 7a) (e.g., Bonforte and Puglisi, 2006; Bonforte et al., 2007; Battaglia et al., 2011; Chiocci et al., 2011; Apuani et al., 2013; Acocella and Puglisi, 2013; Ruch et al., 2013), was dislocated in just a few days toward the crater area (Fig. 5a and 7b). This event of a reversal dislocation is very rare (Aloisi et al., 2011b; Bruno et al., 2012) and, in this case, it was very fast (Fig. 7). It is well know that the Pernicana – Provenzana fault system represents the northern edge of the eastern flank (Fig. 5a) and, beyond this margin toward the north, the motion of the flank abruptly disappears (e.g., Bonforte and Puglisi, 2006; Bonforte et al., 2011; Barreca et al., 2013; Ruch et al., 2013). It is almost certain that the inversion of dislocation at the eastern flank must have produced an alteration of the hydrothermal circulation, in particular, in the northern and western edge of the flank (Fig. 7b). This evidence could indicate a reduction of the effective normal stress along the Pernicana – Provenzana fault system, induced indirectly by the very fast deflation associated to the "Voragine" paroxysmal episodes. In confirmation of this hypothesis, also Mattia et al. (2015) pointed to the crucial interrelationship between fluids of volcanic origin and aquifers, producing the large scale instability of the eastern flank of Mt. Etna. The authors clearly demonstrated that the strain patterns related to the action of volcanic sources (inflation/deflation cycles) influence the pore pressure of the shallower layers, inducing movements in the eastern flank and, consequently, changing the shallow depth fluid circulation. The close correlation between magma emplacement within the North East Rift, the amount of deformation near the Pernicana fault system and the instability of the eastern flank of Mt. Etna has already been discussed by many authors (e.g., Ruch et al., 2013). In our case, it is noteworthy that typical baselines on the eastern flank near the studied area, for example, the ESAL-ERIP and EMFN-EBAG (Fig. 2c), indicated that until about the 6th of December they increased in length according to the overall volcano deflation due to the "Voragine" paroxysmal episodes. From about the 6th of December, when the "Voragine" magmatic activity finished, the trend recorded at the two baselines changed, indicating the resumption of the typical flank seaward movement (Fig. 7b). In conclusion, the 2015 December seismic activity was the consequence of a mosaic of volcanic and tectonic processes. We believe that the "Voragine" paroxysmal episodes induced fast movements in the eastern flank toward the craters area (Fig. 7b) and that the flank resumed its usual seaward movement after about the 6th of December. This process produced a variation in the fluid circulation with the consequent reduction of the friction along the Pernicana – Provenzana fault system. Successively, the onset of the new phase of inflation (Fig. 7c), producing a positive CSC along the fault system, triggered the faulting processes, releasing the pre-stress cumulated during interseismic period (Fig. 7a), as the consequence of the intrusive dynamics preceding the "Voragine" magmatic activity.

## 6. Conclusions

In this paper, the relationship between the eruptive phenomenon and the faulting process in terms of Coulomb stress changes has been investigated. Our study determined that the four paroxysmal episodes at the "Voragine" crater are not the direct cause of the seismic swarm recorded a few days later. We also demonstrated that the violent magmatic activity destabilized this area, promoting a fast inversion of dislocation in the eastern flank and a consequent variation in the fluid circulation. Therefore, due to the presence of intense hydrothermal activity, the rapid deflation indirectly caused a weakening of the failure surface that was successively activated by the start of the new phase of inflation. In fact, our results of the inflation phase following the 2015 December eruptive episodes indicated positive Coulomb stress changes in the Pernicana – Provenzana fault system, in accordance with the location, depth and focal mechanisms of the recorded seismic swarm. Given this match, we can conclude that the recorded seismicity is compatible with a complex and multicausal stress redistribution inside the volcano edifice.

## References


Acocella, v., Puglisi, G., 2013. How to cope with volcano flank dynamics? A conceptual model behind possible scenarios for Mt. Etna. J. Volcanol. Geotherm. Res. 251, 137–148, http://dx.doi.org/10.1016/j.jvolgeores.2012.06.016 (ISSN 0377-0273).

Aloisi, M., Cocina, O., Neri, G., Orecchio, B., Privitera, E., 2002. Seismic tomography of the crust underneath the Etna volcano, Sicily. Phys. Earth Planet. Inter. 134, 139–155, http://dx.doi.org/10.1016/S0031-9201(02)00153-X.

Aloisi, M., Bonaccorso, A., Cannavò, F., Gambino, S., Mattia, M., Puglisi, G., Boschi, E., 2009. A new dike intrusion style for the Mount Etna May 2008 eruption modelled through continuous tilt and GPS data. Terra Nova 21, 316–321, http://dx.doi.org/10.1111/j.1365-3121.2009.00889.x.

Aloisi, M., Mattia, M., Monaco, C., Pulvirenti, F., 2011a. Magma, faults, and gravitational loading at Mount Etna: the 2002–2003 eruptive period. J. Geophys. Res. 116, B05203, http://dx.doi.org/10.1029/2010JB007909.

Aloisi, M., Mattia, M., Ferlito, C., Palano, M., Bruno, V., Cannavò, F., 2011b. Imaging the multi-level magma reservoir at Mt. Etna volcano (Italy). Geophys. Res. Lett. 38, L16306, http://dx.doi.org/10.1029/2011GL048488.

Alparone, S., Andronico, D., Lodato, L., Sgroi, T., 2003. Relationship between tremor and volcanic activity during the Southeast Crater eruption on Mount Etna in early 2000. J. Geophys. Res. 108, 2241, http://dx.doi.org/10.1029/2002JB001866.

Alparone, S., Cocina, O., Gambino, S., Mostaccio, A., Spampinato, S., Tuvè, T., Ursino, A., 2013. Seismological features of the Pernicana-Provenzana fault system (Mt Etna, Italy) and implications for the dynamics of northeastern flank of the volcano. J. Volcanol. Geotherm. Res. 251, 16–26, http://dx.doi.org/10.1016/j.jvolgeores.2012.03.010.

Alparone, S., Maiolino, V., Mostaccio, A., Scaltrito, A., Ursino, A., Barberi, G., D'Amico, S., Di Grazia, G., Giampiccolo, E., Musumeci, C., Scarfì, L., Zuccarello, L., 2015. Instrumental seismic catalogue of Mt Etna earthquakes (Sicily, Italy): ten years (2000–2010) of instrumental recordings. Annals of Geophysics 58 (4), S0435, http://dx.doi.org/10.4401/ag-6591.

Apuani, T., Corazzato, C., Merri, A., Tibaldi, A., 2013. Understanding Etna flank instability through numerical models. J. Volcanol. Geotherm. Res. 251, 112–126, http://dx.doi.org/10.1016/j.jvolgeores.2012.06.015 (ISSN 0377-0273).

Azzaro, R., 1999. Earthquake surface faulting at Mount Etna volcano (Sicily) and implications for active tectonics. J. Geodyn. 28 (2-3), 193–213, http://dx.doi.org/10.1016/s0264-3707(98)00037-4 (ISSN 0264-3707).

Barberi, G., Cocina, O., Neri, G., Privitera, E., Spampinato, S., 2000. Volcanological inferences from seismic strain tensor computations at Mt. Etna Volcano, Sicily. Bull. Volcanol. 62, 318–330.

Barberi, G., Cocina, O., Maiolino, E., Musumeci, C., Privitera, E., 2004. Insight into Mt. Etna (Italy) kinematic during the 2002–2003 eruption as inferred from seismic stress and strain tensors. Geophys. Res. Lett. 31, L21614, http://dx.doi.org/10.1029/2004GL020918.

Barreca, G., Bonforte, A., Neri, M., 2013. A pilot GIS database of active faults of Mt. Etna (Sicily): A tool for integrated hazard evaluation. J. Volcanol. Geotherm. Res. 251, 170–186, http://dx.doi.org/10.1016/j.jvolgeores.2012.08.013 (ISSN 0377-0273).

Battaglia, M., Di Bari, M., Acocella, V., Neri, M., 2011. Dike emplacement and flank instability at Mount Etna: constraints from a poro-elastic-model of flank collapse. J. Volcanol. Geotherm. Res. 199 (1-2), 153–164, http://dx.doi.org/10.1016/j.jvolgeores.2010.11.005 (ISSN 0377-0273).

Bonaccorso, A., Cianetti, S., Giunchi, C., Trasatti, E., Bonafede, M., Boschi, E., 2005. Analytical and 3D numerical modeling of Mt. Etna (Italy) volcano inflation. Geophys. J. Int. 163 (2), 852–862, http://dx.doi.org/10.1111/j.1365-246X.2005.02777.x.

Bonafede, M., Dragoni, M., Quareni, F., 1986. Displacement and stress fields produced by a centre of dilation and by a pressure source in a viscoelastic half-space: application to the study of ground deformation and seismic activity at Campi Flegrei, Italy. Geophys. J. R. Astron. Soc. 87, 455–485.

Bonanno, A., Palano, M., Privitera, E., Gresta, S., Puglisi, G., 2011. Magma intrusion mechanisms and redistribution of seismogenic stress at Mt. Etna volcano (1997–1998). Terra Nova 23, 339–348, http://dx.doi.org/10.1111/j.1365-3121.2011.01019.x.

Bonforte, A., Puglisi, G., 2006. Dynamics of the eastern flank of Mt. Etna volcano (Italy) investigated by a dense GPS network. J. Volcanol. Geotherm. Res. 153

(3–4), 357–369, http://dx.doi.org/10.1016/j.jvolgeores.2005.12.005 (ISSN 0377-0273).
Bonforte, A., Branca, S., Palano, M., 2007. Geometric and kinematic variations along the active Pernicana fault: implication for the dynamics of Mount Etna NE flank (Italy). J. Volcanol. Geotherm. Res. 160 (1–2), 210–222, http://dx.doi.org/10.1016/j.jvolgeores.2006.08.009 (ISSN 0377-0273).
Bonforte, A., Guglielmino, F., Coltelli, M., Ferretti, A., Puglisi, G., 2011. Structural assessment of mount etna volcano from permanent scatterers analysis. Geochem. Geophys. Geosyst. 12, Q02002, http://dx.doi.org/10.1029/2010GC003213.
Bruno, V., Mattia, M., Aloisi, M., Palano, M., Cannavò, F., Holt, W.E., 2012. Ground deformations and volcanic processes as imaged by CGPS data at Mt. Etna (Italy) between 2003 and 2008. J. Geophys. Res. –Solid Earth 117, B07208, http://dx.doi.org/10.1029/2011JB009114.
Calais, E., Freed, A., Mattioli, G., Amelung, F., Jíonsson, S., Jansma, P., Hong, S.H., Dixon, T., Prepetit, C., Momplaisir, R., 2010. The January 12, Mw 7.0 earthquake in Haiti: context and mechanism from an integrated geodetic study. Nat. Geosci., 7, http://dx.doi.org/10.1038/NGEO992.
Cannavó, F., Arena, A., Monaco, C., 2014. Local geodetic and seismic energy balance for shallow earthquake prediction. J. Seismolog., 1–8, http://dx.doi.org/10.1007/s10950-014-9446-z.
Cauchie, L., Saccorotti, G., Bean, C.J., 2015. Amplitude and recurrence time analysis of LP activity at Mount Etna, Italy. J. Geophys. Res. Solid Earth 120, 6474–6486, http://dx.doi.org/10.1002/2015JB011897.
Chiocci, F.L., Coltelli, M., Bosman, A., Cavallaro, D., 2011. Continental margin large-scale instability controlling the flank sliding of Etna volcano. Earth Planet. Sci. Lett. 305 (1-2), 57–64, http://dx.doi.org/10.1016/j.epsl.2011.02.040 (1 May 2011).
Cocina, O., Neri, G., Privitera, E., Spampinato, S., 1997. Stress tensor computations in the Mount Etna area (southern Italy) and tectonic implications. J. Geodyn. 23, 109–127, http://dx.doi.org/10.1016/S0264-3707(96)00027-0.
Currenti, G., Del Negro, C., Ganci, G., Williams, C.A., 2008. Static stress changes induced by the magmatic intrusions during the 2002–2003 Etna eruption. J. Geophys. Res. 113, B10206, http://dx.doi.org/10.1029/2007JB005301.
Currenti, G., Solaro, G., Napoli, R., Pepe, A., Bonaccorso, A., Del Negro, C., Sansosti, E., 2012. Modeling of ALOS and COSMO-SkyMed satellite data at Mt Etna: implications on relation between seismic activation of the Pernicana fault system and volcanic unrest. Remote Sens. Environ. 125, 64–72, http://dx.doi.org/10.1016/j.rse.2012.07.008 (ISSN 0034-4257).
Davis, P.M., 1986. Surface deformation due to inflation of an arbitrarily oriented triaxial ellipsoidal cavity in an elastic half-space, with reference to Kilauea Volcano, Hawaii. J. Geophys. Res. 91 (B7), 7429–7438, http://dx.doi.org/10.1029/jb091ib07p07429.
Di Grazia, G., Falsaperla, S., Langer, H., 2006. Volcanic tremor location during the 2004 Mount Etna lava effusion. Geophys. Res. Lett. 33, L04304, http://dx.doi.org/10.1029/2005GL025177.
Dragoni, M., Bonafede, M., Boschi, E., 1982. Stress relaxation in the Earth and seismic activity. Rivista del Nuovo Cimento 5 (2), 1–34, http://dx.doi.org/10.1007/BF02740828.
Efron, B., 1982. The Jackknife, Bootstrap and Other Resampling Plans. Society for Industrial and Applied Mathematics, Philadelphia.
Ellis, M., King, G., 1991. Structural control of flank volcanism in continental rifts. Science 254, 839–842, http://dx.doi.org/10.1126/science.254.5033.839.
Ferlito, C., Lanzafame, G., 2010. The role of supercritical fluids in the potassium enrichment of magmas at Mount Etna volcano (Italy). Lithos 119, 642–650, http://dx.doi.org/10.1016/j.lithos.2010.08.006.
Ferlito, C., Viccaro, M., Cristofolini, R., 2009. Volatile-rich magma injection into the feeding system during the 2001 eruption of Mt. Etna (Italy): Its role on explosive activity and change in rheology of lavas. Bull. Volcanol. 71, 1149–1158, http://dx.doi.org/10.1007/s00445-009-0290-x.
Feuillet, N., Cocco, M., Musumeci, C., Nostro, C., 2006. Stress interaction between seismic and volcanic activity at Mt. Etna. Geophys. J. Int. 164, 697–718, http://dx.doi.org/10.1111/j.1365-246X.2005.02824.x.
Gambino, S., 2016. Tilt offset associated with local seismicity: the Mt. Etna January 9, 2001 seismic swarm. Open Geosci. 8 (1), 514–522, http://dx.doi.org/10.1515/geo-2016-0045.
Goldberg, D.E., 1989. Genetic Algorithms in Search, Optimization and Machine Learning. Boston, MA, Kluwer Academic Publishers.
Gonzalez, P.J., Palano, M., 2014. Mt. Etna 2001 eruption: new insights into the magmatic feeding system and the mechanical response of the western flank from a detailed geodetic dataset. J. Volcanol. Geotherm. Res. 274, 108–121, http://dx.doi.org/10.1016/j.jvolgeores.2014.02.001.
Gruppo Analisi Dati Sismici, 2016. Catalogo dei terremoti della Sicilia Orientale – Calabria Meridionale (1999-2016). INGV, Catania http://www.ct.ingv.it/ufs/analisti/catalogolist.php.
Guglielmino, F., Bignami, C., Bonforte, A., Briole, P., Obrizzo, F., Puglisi, G., Stramondo, S., Wegmüller, U., 2011. Analysis of satellite and in situ ground deformation data integrated by the SISTEM approach: the April 3, 2010 earthquake along the Pernicana fault (Mt. Etna – Italy) case study. Earth Planet. Sci. Lett. 312 (3-4), 327–336, http://dx.doi.org/10.1016/j.epsl.2011.10.028 (ISSN 0012-821X).
Gvirtzman, Z., Nur, A., 1999. The formation ofMount Etna as the consequence of slab rollback. Nature 401, 782–785, http://dx.doi.org/10.1038/44555.
Harris, R.A., 1998. Introduction to special section: stress triggers, stress shadows, and implications for seismic hazard. J. Geophys. Res. 103, http://dx.doi.org/10.1029/98JB01576 (B10, 24, 358. 347-24).
Hill, D.P., Pollitz, F., Newhall, C., 2002. Earthquake-volcano interactions. Phys. Today 55, 41–47, http://dx.doi.org/10.1063/1.1535006.
Hirn, A., Nercessian, A., Sapin, M., Ferrucci, F., Wittlinger, G., 1991. Seismic heterogeneity of Mt Etna: structure and activity. Geophys. J. Int. 105, 139–153.
Hirn, A., Nicolich, R., Gallart, J., Laigle, M., Cernobori, L., ETNASEIS Scientific Group, 1997. Roots of Etna volcano in faults of great earthquakes. Earth Planet. Sci. Lett. 148, 171–191, http://dx.doi.org/10.1016/S0012-821X(97)00023-X.
Hyodo, M., Hirahara, K., 2004. GeoFEM kinematic earthquake cycle simulation in southwest Japan. Pure Appl. Geophys. 164, 2069–2090, http://dx.doi.org/10.1007/s00024-004-2549-7.
Jin, S.G., Park, P.K., 2006. Strain accumulation in South Korea inferred from GPS measurements. Earth Planets Space 58 (5), 529–534, http://dx.doi.org/10.1186/BF03351950.
King, R., Bock, Y., 2004. Documentation for the MIT GPS Analysis Software: GAMIT. Mass. Inst. of Technol., Cambridge.
King, G.C.P., Stein, R.S., Lin, J., 1994. Static stress changes and the triggering of earthquakes. Bull. Seismol. Soc. Am. 84, 935–953.
Lahr, J.C., 1989. HYPOELLIPSE/VERSION 2.0: A Computer Program for Determining Local Earthquake Hypocentral Parameters, Magnitude and First Motion Pattern, Open File Rep. U. S. Geol. Surv., Washington, pp. 89–116 (92 pp.).
Lewis, R.M., Torczon, V., 1999. Pattern search algorithms for bound constrained minimization. SIAM J. Optim. 9 (4), 1082–1099.
Marzocchi, W., Casarotti, E., Piersanti, A., 2002. Modeling the stress variations induced by great earthquakes on the largest volcanic eruptions of the 20th century. J. Geophys. Res. 107, http://dx.doi.org/10.1029/2001jb001391.
Mattia, M., Patanè, D., Aloisi, M., Amore, M., 2007. Faulting on the western flank of Mt Etna and magma intrusions in the shallow crust. Terra Nova 19, 1–6, http://dx.doi.org/10.1111/j.1365-3121.2006.00724.x.
Mattia, M., Bruno, V., Caltabiano, T., Cannata, A., Cannavò, F., D'Alessandro, W., Di Grazia, G., Federico, C., Giammanco, S., La Spina, A., Liuzzo, M., Longo, M., Monaco, C., Patanè, D., Salerno, G., 2015. A comprehensive interpretative model of slow slip events on Mt. Etna's eastern flank. Geochem. Geophys. Geosyst. 16, http://dx.doi.org/10.1002/2014GC005585.
McNutt, S.R., 1991. Volcanic tremor. Encyclopedia of Earth System Science, vol. 4. Academic, San Diego, Calif, pp. 9.
McTigue, D.F., 1987. Elastic stress and deformation near a finite sphericalmagma body: resolution of the point source paradox. J. Geophys. Res. 92, 12931–12940, http://dx.doi.org/10.1029/JB092iB12p12931.
Newman, A.V., Dixon, T.H., Gourmelen, N., 2006. A four-dimensional viscoelastic deformation model for long valley caldera, california, between 1995 and 2000. J. Volc. Geotherm Res. 150, 244–269, http://dx.doi.org/10.1016/j.jvolgeores.2005.07.017.
Nostro, C., Stein, R.S., Cocco, M., Belardinelli, M.E., Marzocchi, W., 1998. Two-way coupling between Vesuvius eruptions and southern Apennine earthquakes (Italy) by elastic stress transfer. J. Geophys. Res. 103(B10 (24), http://dx.doi.org/10.1029/98JB00902 (487-24 504).
Obrizzo, F., Pingue, F., Troise, C., De Natale, G., 2001. Coseismic displacements and creeping along the Pernicana fault (Etna, Italy) in the last 17 years: a detailed study of a tectonic structure on a volcano. J. Volcanol. Geotherm. Res. 109 (1–3), 109–131, http://dx.doi.org/10.1016/s0377-0273(00)00307-3 (ISSN 0377-0273).
Palano, M., Aloisi, M., Amore, M., Bonforte, A., Calvagna, F., Cantarero, M., Consoli, O., Consoli, S., Guglielmino, F., Mattia, M., Puglisi, B., Puglisi, G., 2006. Kinematics and strain analyses of the eastern segment of the Pernicana fault (Mt. Etna, Italy) derived from geodetic techniques (1997–2005). Ann. Geophys. 49, 1105–1117, http://dx.doi.org/10.4401/ag-3103.
Palano, M., Puglisi, G., Gresta, S., 2008. Ground deformation patterns at Mt. Etna from 1993 to 2000 from joint use of InSAR and GPS techniques. J. Volcanol. Geotherm. Res. 169, 99–120, http://dx.doi.org/10.1016/j.jvolgeores.2007.08.014.
Palano, M., Gresta, S., Puglisi, G., 2009. Time-dependent deformation of the eastern flank of Mt. Etna: after-slip or viscoelastic relaxation? Tectonophysics 473 (3–4), 300–311, http://dx.doi.org/10.1016/j.tecto.2009.02.047.
Palano, M., 2016. Episodic slow slip events and seaward flank motion at Mt. Etna volcano (Italy). J. Volcanol. Geotherm. Res. 324 (15), 8–14, http://dx.doi.org/10.1016/j.jvolgeores.2016.05.010 (September 2016, ISSN 0377-0273).
Patanè, D., Privitera, E., Gresta, S., Alparone, S., Akinci, A., Barberi, G., Chiaraluce, L., Cocina, O., D'Amico, S., De Gori, P., Di Grazia, G., Falsaperla, S., Ferrari, F., Gambino, S., Giampiccolo, E., Langer, H., Maiolino, V., Moretti, M., Mostaccio, A., Musumeci, C., Piccinini, D., Reitano, D., Scarfì, L., Spampinato, S., Ursino, A., Zuccarello, L., 2003. Seismological constraints for the dyke emplacement of the July-August 2001 lateral eruption at Mt. Etna volcano, Italy. Ann. Geophys. 46, 599–608, http://dx.doi.org/10.4401/ag-6302.
Patanè, D., Mattia, M., Aloisi, M., 2005. Shallow intrusive processes during 2002–2004 and current volcanic activity on Mt. Etna. Geophys. Res. Lett. 32, L06302, http://dx.doi.org/10.1029/2004GL021773.
Privitera, E., Bonanno, A., Gresta, S., Nunnari, G., Puglisi, G., 2012. Triggering mechanisms of static stress on Mount Etna volcano. An application of the boundary element method. J. Volcanol. Geotherm. Res. 245-246, 149–158, http://dx.doi.org/10.1016/j.jvolgeores.2012.08.012.
Pulvirenti, F., Aloisi, M., Jin, S., 2016. Time-dependent Coulomb stress changes induced by the 2002–2003 Etna magmatic intrusions and implications on following seismic activities. J. Volcanol. Geotherm. Res., http://dx.doi.org/10.1016/j.jvolgeores.2016.11.001.

Reasenberg, P.A., Oppenheimer, D., 1985. FPFIT, FPPLOT and FPPAGE: Fortran Computer Progams for Calculating and Displaying Earthquake Fault-plane Solutions, Open File Rep. U. S. Geol. Surv., Washington, pp. 85–379 (109 pp).
Reasenberg, P.A., Simpson, R.W., 1992. Response of regional seismicity to the static stress change produced by the Loma Prieta earthquake. Science 255 (5052), 1687–1690, http://dx.doi.org/10.1126/science.255.5052.1687.
Ruch, J., Pepe, S., Casu, F., Solaro, G., Pepe, A., Acocella, V., Neri, M., Sansosti, E., 2013. Seismo-tectonic behavior of the Pernicana Fault System (Mt Etna): A gauge for volcano flank instability? J. Geophys. Res. Solid Earth 118, 4398–4409, http://dx.doi.org/10.1002/jgrb.50281.
Siniscalchi, A., Tripaldi, S., Neri, M., Giammanco, S., Piscitelli, S., Balasco, M., Behncke, B., Magrì, C., Naudet, V., Rizzo, E., 2010. Insights into fluid circulation across the Pernicana Fault (Mt. Etna, Italy) and implications for flank instability. J. Volcanol. Geotherm. Res. 193 (1–2), 137–142, http://dx.doi.org/10.1016/j.jvolgeores.2010.03.013 (ISSN 0377-0273).
Siniscalchi, A., Tripaldi, S., Neri, M., Balasco, M., Romano, G., Ruch, J., Schiavone, D., 2012. Flank instability structure of Mt. Etna inferred by a magnetotelluric survey. J. Geophys. Res. 117, B03216, http://dx.doi.org/10.1029/2011JB008657.
Stein, R.S., 1999. The role of stress transfer in earthquake occurrence. Nature 402, 605–609, http://dx.doi.org/10.1038/45144.
Thatcher, W., Savage, J.C., 1982. Triggering of large earthquakes by magma-chamber inflation, Izu Peninsula, Japan. Geology 10 (12), 637–640, http://dx.doi.org/10.1130/0091-7613.
Tiampo, K.F., Rundle, J.B., Fernandez, J., Langbein, J.O., 2000. Spherical and ellipsoidal volcanic sources at Long Valley caldera, California, using a genetic algorithm inversion technique. J. Volcanol. Geotherm. Res. 102, 189–206, http://dx.doi.org/10.1016/S0377-0273(00)00185-2.
Toda, S., Stein, R.S., Sagiya, T., 2002. Evidence from the 2000 CE Izu islands earthquake swarm that stressing rate governs seismicity. Nature 419, 58–61, http://dx.doi.org/10.1038/nature00997.
Toda, S., Stein, R.S., Lin, J., 2011. Widespread seismicity excitation throughout central Japan following the 2011 M = 9.0 Tohoku earthquake and its interpretation by Coulomb stress transfer. Geophys. Res. Lett. 38, 7, http://dx.doi.org/10.1029/2011GL047834.
Walter, T.R., Amelung, F., 2004. Influence of volcanic activity at Mauna Loa, Hawaii, on earthquake occurrence in the Kaoiki Seismic Zone. Geophys. Res. Lett. 31, L07622, http://dx.doi.org/10.1029/2003GL019131.
Williams, C.A., Wadge, G., 2000. An accurate and efficient method for including the effects of topography in three-dimensional elastic models of ground deformation with applications to radar interferometry. J. Geophys. Res. 105 (B4), 8103–8120, http://dx.doi.org/10.1029/1999jb900307.
Xu, C., Wang, J., Li, Z., Drummond, J., 2010. Applying the Coulomb failure function with an optimally oriented plane to the 2008 Mw 7.9 Wenchuan earthquake triggering. Tectonophysics, ume 491 (1–4), 119–126, http://dx.doi.org/10.1016/j.tecto.2009.09.019 (ISSN 0040-1951).
Yang, X.M., Davis, P.M., Dieterich, J.H., 1988. Deformation from inflation of a dipping finite prolate spheroid in an elastic half-space as a model for volcanic stressing. J. Geophys. Res. 93, 4249–4257.